THE JOURNAL OF BIOLOGICAL CHEMISTRY
Vol. 279, No. 32, Issue of August 6, pp. 33447–33455, 2004
Printed in U.S.A.

Unique Features of the *sodC*-encoded Superoxide Dismutase from *Mycobacterium tuberculosis*, a Fully Functional Copper-containing Enzyme Lacking Zinc in the Active Site*

Received for publication, April 28, 2004, and revised form, May 17, 2004
Published, JBC Papers in Press, May 23, 2004, DOI 10.1074/jbc.M404699200

Laura Spagnolo,[a,b,c] Imre Törő,[a,b,d] Melania D'Orazio,[e] Peter O'Neill,[f] Jens Z. Pedersen,[e] Oliviero Carugo,[g,h] Giuseppe Rotilio,[e] Andrea Battistoni,[e,i] and Kristina Djinović-Carugo[a,j]

From the [a]Structural Biology Laboratory, ELETTRA, Sincrotrone Trieste, and the [g]National Laboratory Technologie Avanzate e nano-SCienza, Istituto Nazionale per la Fisica della Materia, Area Science Park, 34012 Basovizza, Trieste, Italy, the [e]Department of Biology, University of Rome Tor Vergata and Istituto Nazionale per la Fisica della Materia, Via della Ricerca Scientifica, 00133 Rome, Italy, the [f]Radiation and Genome Unit, Medical Research Council, Chilton, Didcot, Oxon OX11 0RD, United Kingdom, and the [h]Department of General Chemistry, University of Pavia, via Taramelli 12, 27100 Pavia, Italy

The *sodC*-encoded *Mycobacterium tuberculosis* superoxide dismutase (SOD) shows high sequence homology to other members of the copper/zinc-containing SOD family. Its three-dimensional structure is reported here, solved by x-ray crystallography at 1.63-Å resolution. Metal analyses of the recombinant protein indicate that the native form of the enzyme lacks the zinc ion, which has a very important structural and functional role in all other known enzymes of this class. The absence of zinc within the active site is due to significant rearrangements in the zinc subloop, including deletion or mutation of the metal ligands His^{115} and His^{123}. Nonetheless, the enzyme has a catalytic rate close to the diffusion limit; and unlike all other copper/zinc-containing SODs devoid of zinc, the geometry of the copper site is pH-independent. The protein shows a novel dimer interface characterized by a long and rigid loop, which confers structural stability to the enzyme. As the survival of bacterial pathogens within their host critically depends on their ability to recruit zinc in highly competitive environments, we propose that the observed structural rearrangements are required to build up a zinc-independent but fully active and stable copper-containing SOD.

Tuberculosis is the major cause of death in the world due to infection with a single microbial agent (1). To ultimately combat this disease, concerted international efforts have been undertaken concerning the structural genomics of its etiological agent, *Mycobacterium tuberculosis* (2).[1] *M. tuberculosis* is a facultative intracellular pathogen capable of persisting in the highly oxidative environment of macrophages due to its resistance to the reactive oxygen and nitrogen species generated by phagocytic cells as part of their antimicrobial response (3). The resistance of *M. tuberculosis* to such reactive molecules is mediated by specific components of the cell wall, such as phenolic glycolipids and cyclopropanated mycolic acids, as well as by many mycobacterial antioxidant enzymes, including the two superoxide dismutases (SODs)[2] encoded by the *sodA* and *sodC* genes.

SODs are widely distributed enzymes that are classified according to the metal cofactors involved in the redox reaction, which catalyze the disproportionation of the superoxide radical (O_2^-) into molecular oxygen (O_2) and hydrogen peroxide (H_2O_2) (4). As the investigation of the strategies used by *M. tuberculosis* to withstand the toxicity of reactive oxygen species may be considered of interest for the development of novel anti-tubercular strategies, several studies have been focused on the role and structure of mycobacterial SODs. *M. tuberculosis sodA* encodes an iron-containing SOD that is actively secreted to inhibit the host responses to mycobacterial infections (5). The structure of this enzyme is very similar to that of other iron- or manganese-containing bacterial SODs (6). On the other hand, *sodC* encodes a membrane-bound enzyme (7) that helps *M. tuberculosis* to survive in macrophages that generate a robust oxidative burst (8). This is in agreement with growing observations showing that *sodC*-null mutants of several pathogens are attenuated in animal models (9). An additional reason to consider the *sodC*-encoded SOD (hereafter referred to as MtSOD) to be important for the protection of *M. tuberculosis* from reactive oxygen species generated by macrophages is that *sodC* is upregulated upon entry into human macrophages, when superoxide production by NADPH oxidase is expected to be very high (7). In contrast, transcription of *sodC* is repressed during mycobacterial non-replicating persistence in mice, when phagocytic NADPH oxidase activity drops to very low levels (10).

* This work was supported in part by a Murst-Cofin grant (to A. B.). The costs of publication of this article were defrayed in part by the payment of page charges. This article must therefore be hereby marked "*advertisement*" in accordance with 18 U.S.C. Section 1734 solely to indicate this fact.

The atomic coordinates and structure factors (code 1PZS) have been deposited in the Protein Data Bank, Research Collaboratory for Structural Bioinformatics, Rutgers University, New Brunswick, NJ (http://www.rcsb.org/).

[b] Both authors contributed equally to this work.

[c] Recipient of a Scuola Internazionale Superiore di Studi Avanzati postdoctoral fellowship. Present address: Inst. of Cancer Research, London SW3 6JB, UK.

[d] Recipient of a long term postdoctoral fellowship from the European Molecular Biology Organization (Heidelberg, Germany) and a Training and Research in Italian Laboratories fellowship from the International Centre of Theoretical Physics (Trieste, Italy).

[i] To whom correspondence may be addressed. Tel.: 39-06-7259-4372; Fax: 39-06-7259-4311; E-mail: andrea.battistoni@uniroma2.it.

[j] To whom correspondence may be addressed: Structural Biology Lab., ELETTRA, Sincrotrone Trieste, Area Science Park, S. S. 14, Km. 163.5, 34012 Basovizza, Trieste, Italy. Tel.: 39-040-375-8059; Fax: 39-040-375-8029; E-mail: kristina.djinovic@elettra.trieste.it.

[1] Available at www.doe-mbi.ucla.edu/TB/ and www.pasteur.fr/recherche/X-TB/.

[2] The abbreviations used are: SOD, superoxide dismutase; MtSOD, *M. tuberculosis* superoxide dismutase; Cu,Zn-SOD, copper/zinc-containing superoxide dismutase; ApSOD, *A. pleuropneumoniae* superoxide dismutase; XlSOD, *X. laevis* superoxide dismutase; MES, 4-morpholineethanesulfonic acid; MOPS, 4-morpholinepropanesulfonic acid.

Copper/zinc-containing SODs (Cu,Zn-SODs) are characterized by a conserved arrangement of the redox center, where Cu^{2+} is coordinated by four histidines, and the zinc ion is bound by three histidines and one aspartic acid. The two metal ions are simultaneously coordinated by a common histidine ligand (termed the "histidine bridge" or the "bridging imidazolate"), forming a structural motif found so far only in Cu,Zn-SODs (11). The copper ion is cyclically reduced and oxidized during successive encounters with the substrate (12), whereas the zinc ion has a very important structural role (13) and has also been shown to finely modulate the redox properties of the copper ion (14). Although its primary sequence shows some unusual features, the *sodC*-encoded enzyme is classified as a Cu,Zn-SOD due to its sequence homology to other enzymes belonging to this family (2, 15).

Here, we present the crystal structure of the *sodC*-encoded enzyme from *M. tuberculosis* at 1.63-Å resolution, which was solved by the molecular replacement method using yeast Cu,Zn-SOD as a search model. Albeit this enzyme shows clear structural homology to the other enzymes of the Cu,Zn-SOD family, it was found to be fully functional despite the lack of the zinc ion in the active site and consequent structural rearrangements. The structure additionally presents a novel intersubunit interface distinct from those so far observed for dimer interactions in eukaryotic and prokaryotic Cu,Zn-SODs.

EXPERIMENTAL PROCEDURES

MtSOD Expression and Purification—Soluble recombinant MtSOD was purified from *Escherichia coli* 71/18 cells harboring plasmid pΔCysMycSOD (7). Cells were grown in LB broth supplemented with 125 μM $CuSO_4$, and MtSOD expression was induced in the early logarithmic phase by the addition of 4 μM isopropyl-β-D-thiogalactopyranoside. Three hours after induction, cells were harvested by centrifugation, and the periplasmic proteins were extracted as described previously (16). Proteins were dialyzed against 20 mM Tris-HCl (pH 7.0), loaded onto a HiLoad 16/10 Q-Sepharose fast protein liquid chromatography column (Amersham Biosciences), and fractionated with a 0–150 mM NaCl linear gradient. Fractions containing MtSOD were concentrated and injected onto a HiLoad 16/60 Superdex 75 fast protein liquid chromatography gel filtration column (Amersham Biosciences) equilibrated with 20 mM Tris-HCl (pH 7.0) and 0.15 M NaCl. MtSOD eluted in a single peak with an apparent molecular mass close to 50 kDa. As a final step, the enzyme was further subjected to ion-exchange chromatography on a HiLoad 16/10 Q-Sepharose column (Amersham-Biotech) using a 0–0.2 M NaCl linear gradient in 20 mM Tris-HCl (pH 7.8). At this stage, the protein appeared to be >95% homogeneous, as judged by SDS-PAGE analysis. Protein concentration was evaluated by the method of Lowry *et al.* (17) using bovine serum albumin as a standard. To determine the metal content of MtSOD, the purified protein was extensively dialyzed against Chelex 100-treated 10 mM phosphate buffer (pH 7.0) and then analyzed by atomic absorption spectroscopy using a PerkinElmer Life Sciences AAnalyst 300 spectrometer equipped with a HGA-800 graphite furnace. The copper content was found to be between 0.6 and 0.8 eq/enzyme subunit depending on the preparations, whereas only a trace amount of zinc was found.

Activity Assays—SOD activity assays as a function of pH and ionic strength were carried out by the pulse radiolysis method (18) as recently described (19).

Spectroscopy—Electronic absorption studies were carried out using a Beckman Coulter DU 800 UV-visible spectrophotometer. EPR spectra were recorded at 298 K with a Bruker ESP300 spectrometer operating at 9.82 GHz using a high sensitivity TM_{110} cavity and flat glass capillaries. The protein copper concentration was 1 mM in 20 mM Tris-HCl. The pH titration was carried out by adding small amounts of 1 M NaOH; the pH was determined before and after each EPR measurement using a pH microelectrode.

Demetallation/Remetallation of MtSOD—To remove metals from MtSOD, 10 mg/ml samples of the enzyme were initially dialyzed for 24 h at 4 °C against 50 mM sodium acetate buffer (pH 3.8) and 2 mM EDTA and then for 24 h against 50 mM sodium acetate (pH 3.8) and 0.1 M NaCl to remove EDTA. These samples were subsequently dialyzed twice against 50 mM sodium acetate buffer (pH 5.0) and finally against 50 mM sodium acetate buffer (pH 5.5). The complete absence of zinc and copper ions was verified by atomic absorption analysis. To investigate the presence of a functional zinc-binding site, $CoCl_2$ or $ZnCl_2$ was added to the copper-reconstituted enzyme, and metal uptake was checked by monitoring changes in the electronic and EPR spectra and by atomic absorption analyses.

Crystallization—Crystallization setups utilizing the hanging drop vapor diffusion method produced well diffracting crystals in the form of plates in a couple of days. For all crystallization experiments, a single batch of MtSOD preparation with a concentration of 10 mg/ml was used. The optimal crystallization condition is 30% polyethylene glycol 4000, 200 mM ammonium sulfate, 20 mM $ZnCl_2$, and 100 mM Tris (pH 8.2).

Data Collection and Data Processing—Prior to data collection, the crystals were transferred to a cryoprotecting solution containing 20% glycerol and a slightly elevated polyethylene glycol 4000 concentration. The crystals were flash-frozen and kept under a 100 K dry nitrogen stream during data acquisition. The diffraction data were collected at the ID13 microfocus beamline of the European Synchrotron Radiation Facility, where the fine focus of the x-ray beam allows collection of data from small but perfect regions of slightly imperfect crystals. 180 rotation images with a 1° oscillation angle were collected in one pass without significant overloads in the low resolution regime. The data were integrated and scaled by XDS (20) and were converted to CCP4 MTZ format. Statistics of data collection are shown in Table I.

Structure Solution and Refinement—The crystal structure of MtSOD was solved by molecular replacement utilizing the structure of a Cu,Zn-SOD from yeast (Protein Data Bank code 1JCV) as a search model. The first solution peak of the rotation function in MOLREP (21) was identified as the correct solution with nearly 2-fold peak height compared with the rest. The molecular replacement solution was used as input to the ARP/wARP program suite (22) without any modification to the template sequence. In the first step, 25 cycles of the protocol "Improvement of Model by Atom Update and Refinement" were applied, followed by 50 cycles of refinement with automatic main chain tracing at the end of each 10 refinement cycles. This procedure resulted in a protein structure of 162 residues of two peptide chains. The correct side chains were unambiguously docked by the helper program GUISIDE. Nine additional residues were manually added to the structure. The refinement of the structure was carried out with REFMAC Version 5.1.24 (23) as included in CCP4 Version 4.2.2 (24). Water molecules were added to the structure by ARP/wARP (CCP4 version) after each of five REFMAC cycles. The refinement of the structure was completed when correct geometry and good correlation with diffraction data had been reached as judged from root mean square deviation from ideal geometry, R- and free R-factors, respectively. The structure was validated prior to submission to the Protein Data Bank using PROCHECK (25) and SFCheck (26). Details of refinement statistics are shown in Table I.

Structure-based Alignment and Structural Comparisons—The structure-based alignment was generated with the program TOPP from the CCP4 program suite (27) using an MtSOD monomer on which the structures of *Actinobacillus pleuropneumoniae* SOD (ApSOD) and *Xenopus laevis* SOD (XlSOD) monomers were superimposed. The program TOPP was set to the default parameters, counting a pair of residues as matching residues if there are at least three residues in a consecutive fragment of which C-α atoms are within 3.8 Å in the superimposed structures.

Structural comparisons and classifications were performed with the STRUCLA metaserver (28). A default distance cutoff of 3.5 Å was used to define atomic equivalencies after optimal superposition. Phylogenetic trees were built and analyzed with TreeView (29).

RESULTS

The *sodC* gene of *M. tuberculosis* encodes an SOD of 240 residues (Swiss-Prot accession number P96278), which is post-translationally modified by cleaving a 32-amino acid long leader peptide from the N terminus. The mature protein is anchored to the bacterial membrane via a glyceride/fatty acid lipid attached to its N-terminal cysteine residue (7). To facilitate the biochemical characterization of the enzyme, the mature protein was expressed as a periplasmic soluble form in *E. coli*. The numbering of the sequence starts from the N-terminal cysteine of the mature protein as shown in Fig. 1, and this numbering scheme is used throughout.

Crystallographic Analysis—The refined model of MtSOD reported here consists of one monomer containing a total of 170 residues, one copper ion, and 252 water molecules. No zinc ion

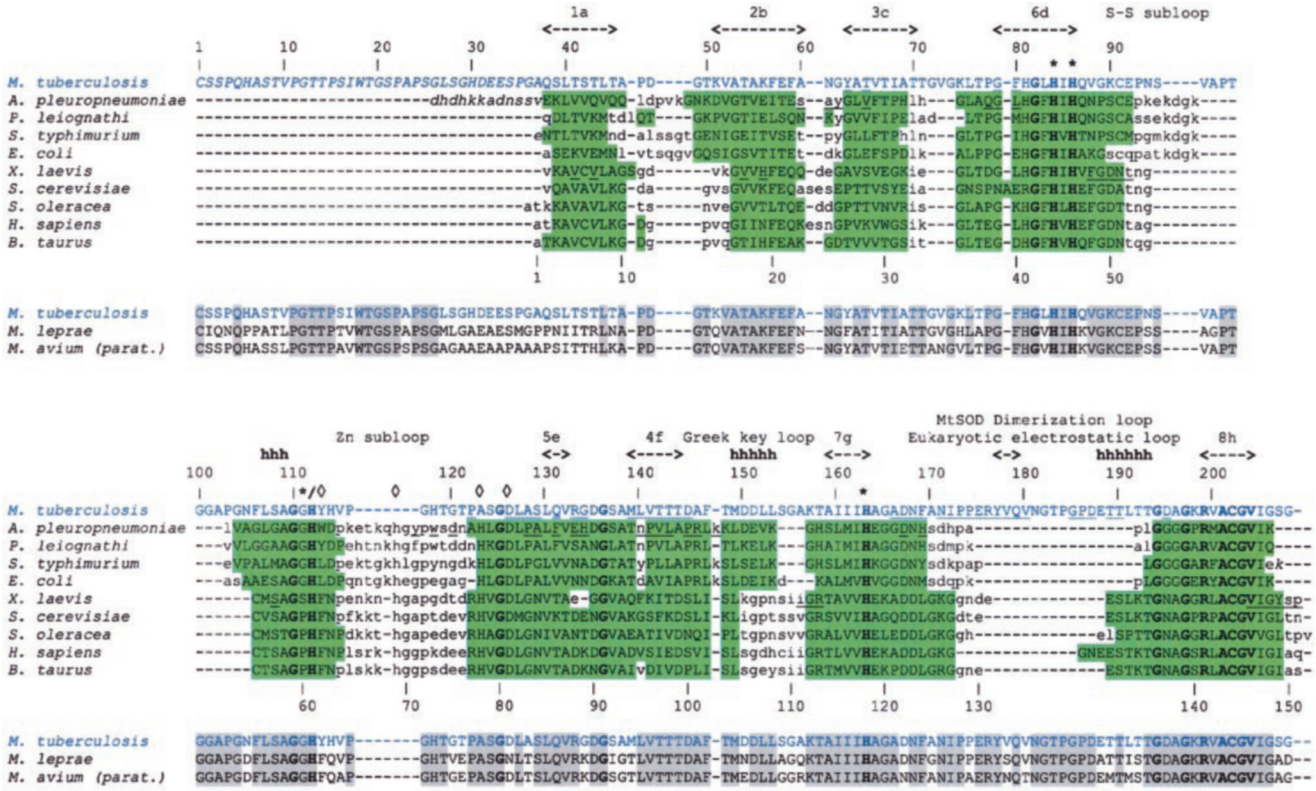

FIG. 1. **Structure-based sequence alignment of MtSOD and all Cu,Zn-SODs for which structures have been solved up to now.** Residues not present in the aligned crystal structures are shown in *italics*. Structurally superimposable residues are in *uppercase letters* and highlighted in *green*. Residues involved in the dimer interface of *M. tuberculosis*, *A. pleuropneumoniae*, and *X. laevis* SODs identified by the Protein-Protein Interaction server are *underlined*. Secondary structural elements relative to MtSOD are indicated as *dashed double-headed arrows* (β-sheet) and *hhh* (α-helix). The homologous sequences from *M. tuberculosis, M. leprae*, and *M. avium* ssp. *paratuberculosis* (*parat.*) are shown in a sequence-based alignment generated with ClustalW software (55), with gaps introduced to fit the structure-based alignment and *gray* highlighting of identical residues. Universally conserved residues in *all* sequences shown are in *boldface*. MtSOD numbering is shown above its sequence, and bovine numbering below its sequence. Copper-binding (*) and zinc-binding (◊) residues are indicated.

is present in the crystal structure, although Zn^{2+} had been added to the crystallization mixture. The occupancy of the copper ion was set to 0.75 in agreement with σ_A-weighted ($2F_o - F_c$ and $F_o - F_c$) difference density maps. The crystallographic *R*-factor and free *R*-factor for the refined model are 0.150 and 0.190 for the diffraction data in the 27.95- to 1.63-Å resolution range (Table I). The electron density is clearly defined for residues 38–208, whereas residues 1–37 are not visible in the electron density.

Overall Structure and Comparison with Other Cu,Zn-SOD Structures—MtSOD adopts the eight-stranded antiparallel β-barrel with Greek key topology that is typical of both eukaryotic and prokaryotic Cu,Zn-SODs (30). Such a topological organization allows the closure of the β-barrel through two external crossing loops (Fig. 2*A*). Residue 38 is at the beginning of β-strand 1a of the classical Cu,Zn-SOD scaffold (Figs. 1 and 2*A*). The preceding 37 residues are probably not ordered due to the extreme flexibility of this N-terminal region, which is involved in the connection to the membrane (7). The structure-based alignment shown in Fig. 1 and superposition of MtSOD with ApSOD and XlSOD (Fig. 2*B*) show the special features of the *sodC*-encoded SOD from *M. tuberculosis* with respect to the prokaryotic and eukaryotic SOD enzymes.

Structural comparisons and classifications of MtSOD with representative structures of eukaryotic and prokaryotic Cu,Zn-SODs were performed with the STRUCLA metaserver (28), which makes a consensus phylogenetic analysis (Fig. 2*C*) based on various measures of structural divergence between pairs of three-dimensional models, including PRIDE (31), rmsd_100 (32), the classical root mean square deviation, the Johnson approach (33) and the Grishin procedure (34). Two completely independent measurements of structural divergence (PRIDE and rmsd_100) are shown in the Tables II and III. rmsd_100 is the root mean square deviation that would have been observed after optimal superposition if the proteins being compared had 100 residues, and PRIDE is a probability value based on C-α–

TABLE I
Data processing and refinement statistics

Resolution range (outer shell) (Å)	27.95 to 1.63 (1.80 to 1.63)
Completeness (%)	96.0 (87.9)
$\langle I/\sigma I \rangle$	13.5 (5.2)
R_{sym} (%)[a]	6.7 (27.3)
No. reflections	20248
R-factor (%)[b]	15.0
R_{free} (%)[b]	19.0
Correlation coefficient between F_o and F_c	0.969
Ramachandran plot	
Core (allowed) (%)	89.5 (10.5)
r.m.s.d.[c] from ideality	
Bonds (Å)	0.010
Angles	1.36°
No. atoms (*B*-factor) (Å^2)	
Non-H protein atoms	1198 (15.03)
Copper ions	1 (20.75)
Water	272 (31.28)

[a] $R_{sym} = \Sigma_{hkl}\Sigma_i|I_i(hkl) - \langle I(hkl)\rangle|/\Sigma_{hkl}\langle I(hkl)\rangle$, where I_i is the intensity of the *i*th measurement of reflection *hkl* and $\langle I \rangle$ is the average intensity of these *i* reflections.

[b] *R*-factor $= \Sigma_{hkl}|F_o| - k|F_c|/\Sigma_{hkl}|F_o|$, where *k* is a scaling factor. R_{free} is calculated in the same way with 5% of the reflections that were omitted from refinement.

[c] Root mean square deviation.

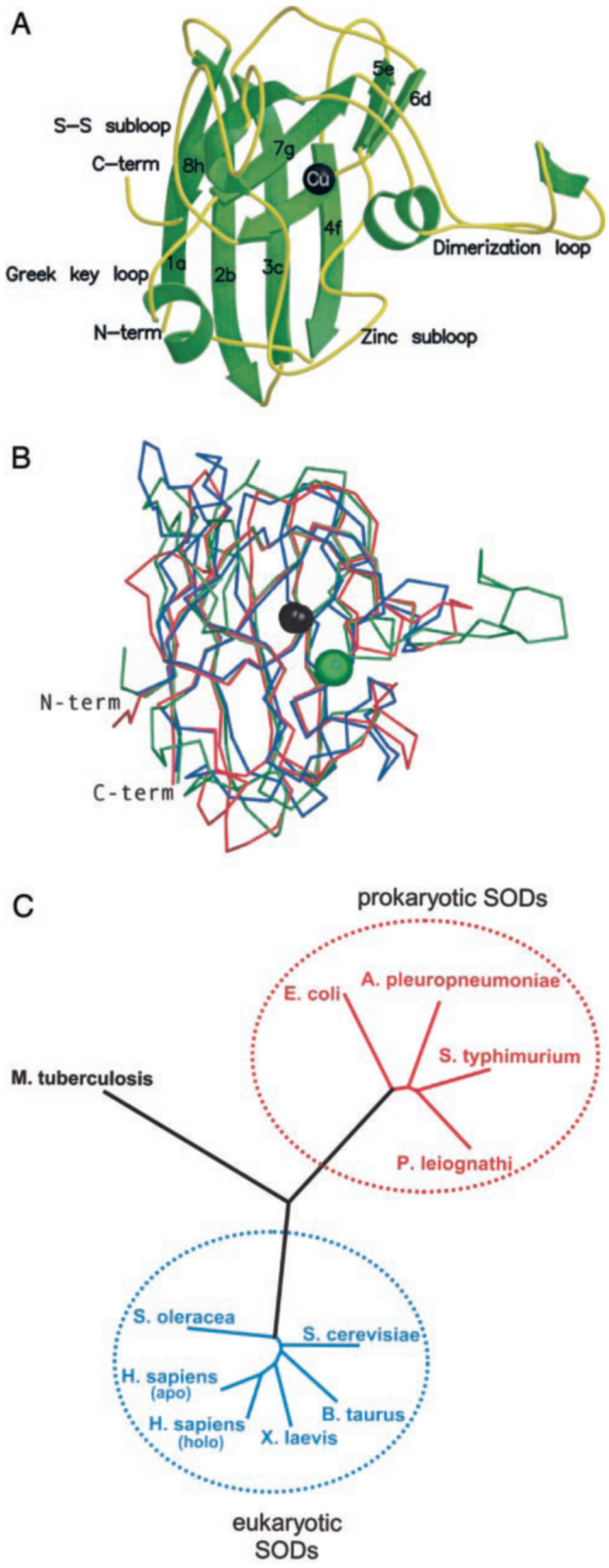

FIG. 2. *A*, schematic view of the tertiary structure of MtSOD showing the characteristic structural elements of all Cu,Zn-SODs and the dimerization loop, a unique feature of MtSOD. Helices and β-strands are *green*, and loops are *yellow*. The figure was prepared by Molscript (56) and Rastrer3d (57). *B*, superposition of MtSOD (*green*), ApSOD (*blue*), and XlSOD (*red*) made by TOPP. The superimposed proteins are oriented according to *A*. The figure was prepared by PyMOL (58). *C*, phylogenetic tree of the SODs from prokaryotes, eukaryotes, and *M. tuberculosis* obtained by the consensus approach implemented in the STRUCLA metaserver. *term*, terminus.

TABLE II
Average PRIDE values (standard deviations on the last digit in parentheses) obtained by comparing the SODs of prokaryotes, eukaryotes, and M. tuberculosis

PRIDE values	Prokaryotic	Eukaryotic	*M. tuberculosis*
Prokaryotic	0.89 (4)	0.77 (2)	0.63 (6)
Eukaryotic	0.77 (2)	0.96 (1)	0.76 (2)
M. tuberculosis	0.63 (6)	0.76 (2)	

TABLE III
Average rmsd_100 values (standard deviations on the last digit in parentheses) obtained by comparing the SODs of prokaryotes, eukaryotes, and M. tuberculosis

rmsd_100 values	Prokaryotic	Eukaryotic	*M. tuberculosis*
Prokaryotic	0.27 (2)	0.70 (1)	0.60 (2)
Eukaryotic	0.70 (1)	0.23 (1)	0.63 (1)
M. tuberculosis	0.60 (2)	0.63 (1)	

C-α distance comparison. The perfect matching between three-dimensional structures of two proteins is associated with values for rmsd_100 of 0.0 and for PRIDE of 1.00. Large rmsd_100 values indicate very divergent models as well as PRIDE values close to 0.0.

Active Site and Zinc Subloop—The active site of Cu,Zn-SODs is located at the bottom of an ~7-Å long protein channel built by residues belonging to the S–S subloop and residues belonging to the electrostatic loop. In MtSOD, the copper ion is coordinated by His^{84}, His^{86}, His^{163}, and a water molecule. The distances of the copper ion from these residues are 2.07 Å (Cu–His^{84} N-δ1), 2.05 (Cu–His^{86} N-ϵ2), 2.04 Å (Cu–His^{163} N-ϵ2), and 1.93 Å (Cu–H_2O), whereas the fourth putative ligand (His^{112} N-ϵ2), which corresponds to the bridging ligand present in all the other Cu,Zn-SODs, is situated 3.29 Å from the copper ion (Fig. 1 and 3*A*).

Mutations and deletions of conserved residues involved in zinc coordination were analyzed by superposition of zinc subloops (Fig. 3*B*) in copper/zinc-containing ApSOD and MtSOD. Two conserved zinc-binding histidine residues are missing in MtSOD: position 123 hosts an Ala, whereas His^{69} (bovine numbering) is lost because of a seven-residue deletion in the zinc subloop. This deletion brings about structural rearrangements that involve also the second coordination sphere of the catalytic metal.

Dimer Architecture—All eukaryotic Cu,Zn-SODs have a tight and stable dimeric structure based on a conserved subunit interface that is formed by 19 residues coming from β-strands 1a, 2b, and 8h, from the S–S subloop, and from the Greek key subloop, and by the C-terminal region (Fig. 2*A*). The quaternary structure assembly in prokaryotic Cu,Zn-SODs is entirely different and is based on 18 residues provided by β-strands 4f and 5e and by loops 2/3 and 7/8 (Fig. 4, *A* and *B*). Similar to other SODs, MtSOD is a functional dimer as shown by size-exclusion chromatography (see "Experimental Procedures"). As the asymmetric unit of MtSOD crystals contains only one molecule, the dimer model was therefore generated by a symmetry operation on the monomer around the 2-fold symmetry axis (Fig. 4, *A* and *B*). The accessible surface area involved in the formation of the dimers of MtSOD, ApSOD, and XlSOD was calculated using the Protein-Protein Interaction server (35). The MtSOD dimer has a buried surface area of 1637 $Å^2$, which represents 18.9% of the total surface area of a subunit. These values decrease to nearly half for the ApSOD and XlSOD dimers (Table IV). As with ApSOD and XlSOD, hydrophobic interactions play an important role in the stabilization of the dimer, as 62.3% of the interface residues are non-polar amino acids (Table IV).

Catalytic Activity and Electrostatics of MtSOD—The cata-

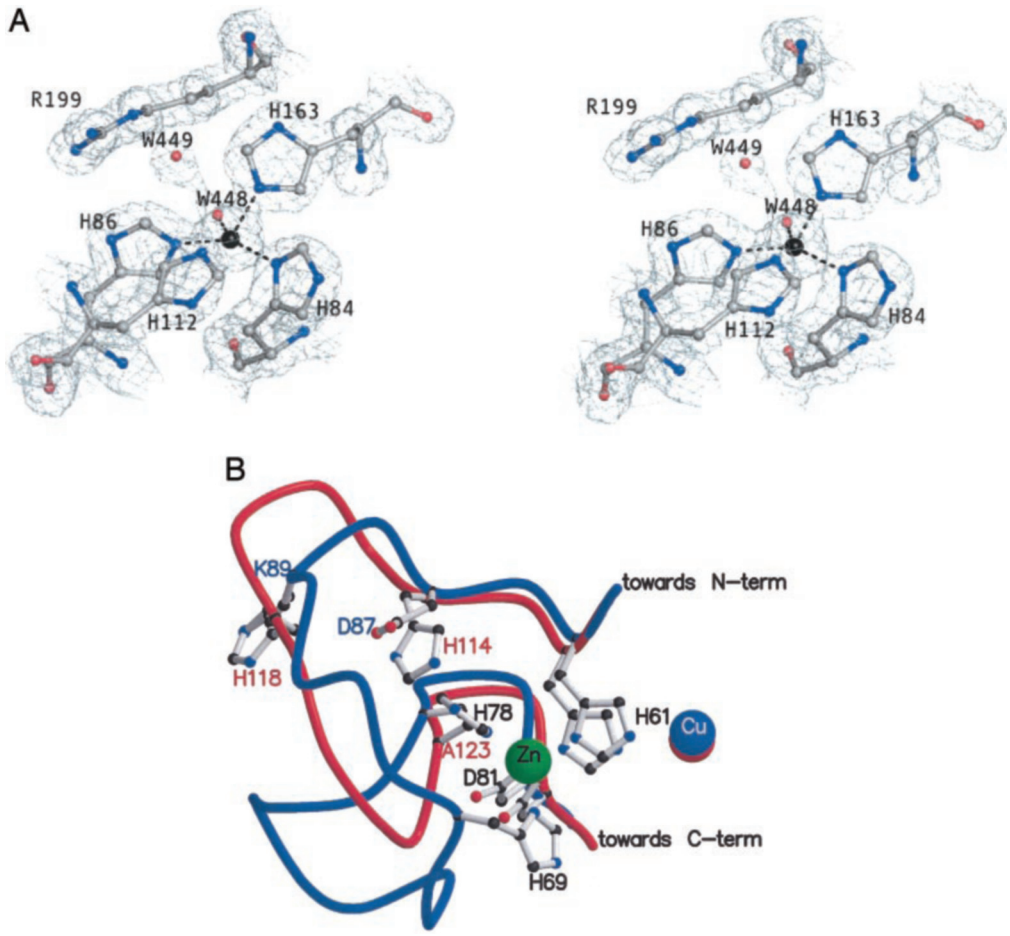

FIG. 3. *A*, active center of MtSOD showing the copper ion and its coordinating residues as well as electron density of a $2F_o - F_c$ map contoured at the 1.4σ level. Besides the residues involved in coordination (connected to copper with *dashed lines*), the universally conserved Arg^{199} (Arg^{141} in bovine SOD), the "bridging" His^{112} (His^{61} in bovine SOD), and a water molecule with connectivity to the copper ligand (*W448*) are shown. The figure was prepared by PyMOL (58). *B*, superposition of MtSOD (*red*) and ApSOD (*blue*) demonstrating the differences between the zinc subloops of mycobacterial and classical bacterial Cu,Zn-SODs. Conserved residues in Cu,Zn-SODs (bovine numbering) are labeled in *black*; residues mutated or unique in MtSOD are labeled in *red*. The zinc subloop of MtSOD is significantly shorter and lacks some of the residues indispensable for zinc binding such as His^{69} and His^{78} (bovine numbering). His^{69} is missing due to deletion of part of the zinc subloop in MtSOD, whereas His^{78} is mutated to Ala^{123} in all mycobacterial SODs. The positions of the two histidine residues (His^{114} and His^{118}) in the short zinc loop of MtSOD exclude zinc binding. The figure was prepared by Molscript (56) and Rastrer3d (57). *term*, terminus.

lytic activity of MtSOD was measured by pulse radiolysis as a function of pH and ionic strength (0.02–0.2 M). Fig. 5*A* shows the pH dependence of the catalytic rate constant for the reaction of superoxide with MtSOD at low ionic strength (0.02 M).

The conservation of a substrate-enzyme electrostatic attraction mechanism is confirmed by activity measurements showing that the catalytic rate of MtSOD is very dependent on increasing the ionic strength (Fig. 5*B*) (36). The slope of the ionic strength dependence of the association rate constant can be taken as an indication of the apparent charge sensed by superoxide. In this case, it is 1.3, significantly lower than that of the SOD from *Salmonella typhimurium* or *Photobacterium leiognathi* (19). Therefore, at ionic strength values close to the physiological range (0.15 M), the difference in activity between MtSOD and the other bacterial enzymes is small.

Mycobacterial SODs do not host charged residues in the S–S subloop or in the dimerization loop (which corresponds to the eukaryotic electrostatic loop). The active site is nevertheless surrounded by an area of positive potential centered on a lysine residue (Lys^{198} in MtSOD) (Fig. 6).

Spectroscopic Analyses—The visible absorption spectrum of purified MtSOD in the 350–750 nm region is shown in Fig. 7*A*. This spectrum was stable in the pH range 6–9 and was not affected by the addition of stoichiometric amounts of zinc. The spectrum of the copper chromophore of the bacterial enzyme displays two bands with maxima at 673 and 355 nm.

The EPR spectrum shows only minor differences with respect to those of typical bacterial Cu,Zn-SODs (Fig. 7*B*). Thus, the absence of Zn^{2+} in MtSOD does not lead to a modified Cu^{2+} ligand arrangement or geometry.

To evaluate the potential ability of MtSOD to bind zinc, we attempted to introduce cobalt into the demetallated protein to form a copper/cobalt-containing SOD derivative. Copper/cobalt-containing SODs maintain the same enzymatic activity (12) and three-dimensional structure (37) of the zinc-containing enzyme and are therefore excellent tools to investigate the properties of the metal cluster by spectroscopic techniques. The addition of a stoichiometric amount of copper to the demetallated protein produced an enzyme with visible and EPR spectra indistinguishable from those of the original protein. The subsequent addition of $CoCl_2$ (from a substoichiometric amount to a 10-fold molar excess) to the copper-reconstituted enzyme dissolved in different buffers in the pH 5.5–7.5 range did not modify the spectral properties of MtSOD.

DISCUSSION

Overall Structure and Comparison with Other Cu,Zn-SOD Structures—The MtSOD structure is characterized by a very

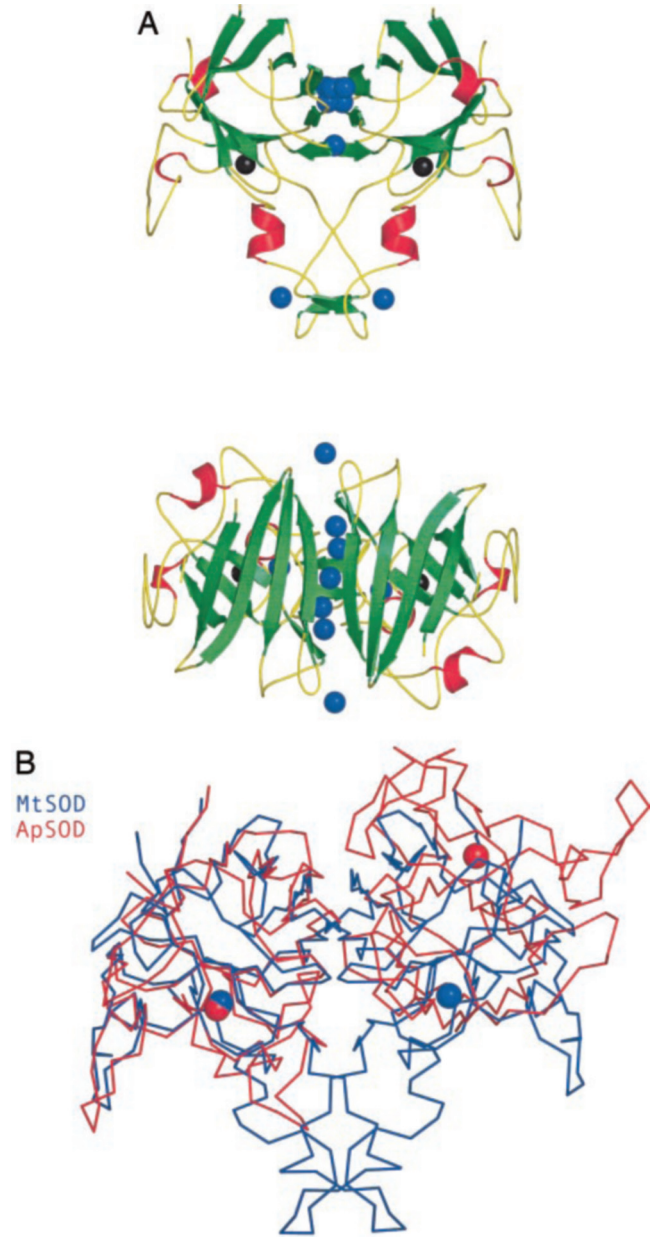

FIG. 4. *A*, schematic view of the tertiary structure of the MtSOD dimer in two orientations. In the *lower part*, the dimer is turned by 90° downwards around the *horizontal axis*. The β-strands are *green*; helices are *red*; and loops are *yellow*. Water molecules bridging subunits by hydrogen bonds are shown as *blue spheres*; the copper ions are shown as *black spheres*. The figure was prepared by PyMOL (58). *B*, superposition of the ApSOD dimer (*red*) on the MtSOD dimer (*blue*) based exclusively on one of the two subunits (*left side*). The figure illustrates the novel dimer architecture of MtSOD compared with the classical bacterial Cu,Zn-SOD arrangement, as found, for example, in ApSOD. The change in the mutual orientation of the subunits in MtSOD (*right side*) results in a completely different dimerization interface.

TABLE IV
Analysis of the dimer interfaces of the three representative SODs from M. tuberculosis, A. pleuropneumoniae, and X. laevis by the Protein-Protein Interaction server

	Interface ASA[a]	Interface ASA	Polar residues	Apolar residues	H-bonds	Salt bridges	HOH
		%	%	%			
MtSOD	1637.59	18.93	37.62	62.30	34	2	14
ApSOD	824.18	10.85	28.93	71.00	2	0	9
XlSOD	684.51	9.41	28.51	71.40	4	0	3

[a] Accessible surface area.

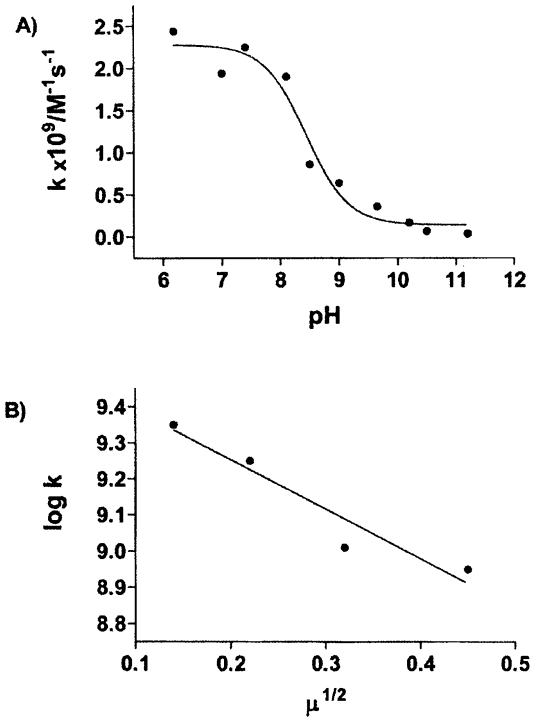

FIG. 5. *A*, plot of the catalytic rate constant (k_{cat}/K_m) of MtSOD as a function of pH. The enzyme was assayed at 20 °C in Tris/MES (up to pH 7.2), in Tris/MOPS (pH 7.0–9.0), and in borate buffer (pH 9.5–12). The concentration of each buffer was calibrated to keep the ionic strength constant at 20 mM. The protein concentration for each sample varied in the range 0.25–0.75 μM. *B*, ionic strength dependence of the catalytic rate constant (k_{cat}/K_m) of MtSOD. Measurements were carried out in Tris/MOPS (pH 7.4). The ionic strength was increased from 0.02 to 0.2 M by the addition of $NaClO_4$ to the sample buffer.

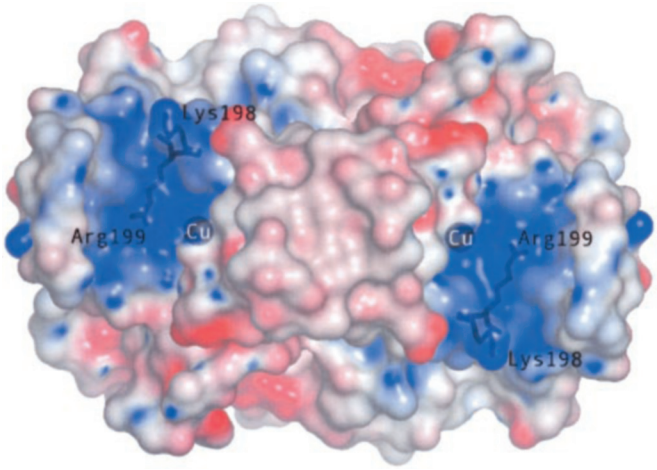

FIG. 6. **Electrostatic potential calculated by APBS (59) mapped on the surface of the MtSOD dimer.** Positive potential at the surface is indicated in *blue*, and negative potential is indicated in *red*. The most positive surface patch of MtSOD belongs to the active center and its close neighborhood, the copper ion, the invariant Arg^{199}, and Lys^{198}, which are highlighted.

distinct distribution of loops with respect to other known Cu,Zn-SODs: the zinc loop is much shorter, whereas a very long loop involved in dimerization (hereafter termed the dimerization loop) connects β-strands 7g and 8h. The conserved residues forming the bacterial electrostatic loop (KDGK) are completely missing, as are the residues of the eukaryotic electrostatic loop (Figs. 1 and 2*A*).

The region that is most stringently conserved in MtSOD is formed by β-strand 8h; six of the eight residues are fully con-

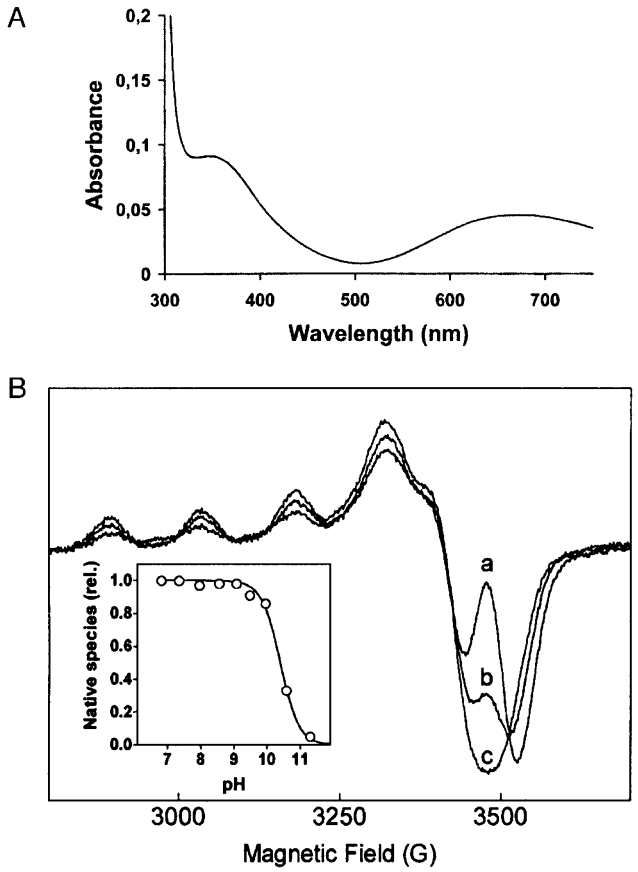

FIG. 7. *A*, visible absorption spectrum of MtSOD. The spectrum of 0.16 mM MtSOD in 10 mM potassium phosphate buffer (pH 7.0) was recorded at 25 °C. *B*, EPR spectra of MtSOD measured at 25 °C. Samples contained 1 mM MtSOD in 10 mM phosphate buffer at pH 11.3 (*spectrum a*), pH 10.6 (*spectrum b*), and pH 8.0 (*spectrum c*). The *inset* shows the relative (*rel.*) fraction of the native enzyme EPR signal ($g_{\parallel}$ = 2.26 and $g_{\perp}$ = 2.05) remaining after incubation at room temperature for 20 min; back-titration from pH 11.3 by the addition of HCl resulted in ~75% recovery (not shown).

served in the nine known structures belonging to both prokaryotic and eukaryotic organisms. Among the conserved residues are Arg^{141} (bovine numbering), close to the active site, and Cys^{144} (bovine numbering), which forms a disulfide bridge with Cys^{51} (bovine numbering) in prokaryotic SODs and with Cys^{55} (bovine numbering) in eukaryotic SODs. Although Cys^{51} of prokaryotes and Cys^{55} of eukaryotes do not superimpose at all in the structures (Fig. 1), they still maintain the same structural role. The very high sequence homology to *Mycobacterium leprae* and *Mycobacterium avium* ssp. *paratuberculosis* (Fig. 1) allows us to extend our structural assumption to the two other known mycobacterial SOD sequences.

From the structural comparisons of MtSOD with representative structures of eukaryotic and prokaryotic Cu,Zn-SODs, it clearly appears that the eukaryotic enzymes cluster together before merging with the cluster of the prokaryotic SODs (Fig. 2*C*). The *M. tuberculosis* enzyme merges with the supercluster of the prokaryotic and eukaryotic proteins, being about equidistant from both the prokaryotic and eukaryotic examples. The rmsd_100 values reported in Table III are, on average, much smaller for prokaryotic-prokaryotic and eukaryotic-eukaryotic comparisons (0.27 and 0.23 Å, respectively). In contrast, the degree of similarity between eukaryotic and prokaryotic proteins (0.70 Å) compares well with that between MtSOD and the prokaryotic and eukaryotic enzymes (0.60 and 0.63 Å, respectively). Analogously, the PRIDE values obtained by comparing prokaryotic and eukaryotic proteins (0.77) match well, on average, with those associated with the comparisons between MtSOD and the eukaryotic and prokaryotic enzymes (0.76 and 0.63, respectively), whereas much higher PRIDE values are obtained within the prokaryotic and eukaryotic clusters (0.89 and 0.96, respectively). This analysis indicates that MtSOD is structurally equally distant from eukaryotic as well as prokaryotic Cu,Zn-SODs.

Active Site and Zinc Subloop—Similar to other Cu,Zn-SODs, the copper coordination in MtSOD is distorted square planar with water as the fifth ligand. The long distance between this bridging residue (His^{112}) and copper (3.29 Å) can be interpreted as a result of the reduction of Cu^{2+} to Cu^{+} during the data collection and is also in agreement with the Cu–His^{61} distance of the chemically reduced bovine enzyme (38–40).

Mutations and deletions of conserved residues involved in zinc coordination in the classical Cu,Zn-SODs (*e.g.* ApSOD) explain the inability of the *M. tuberculosis* enzyme to bind zinc. The histidine residue at position 123 (His^{78} in bovine SOD) is mutated to alanine, whereas His^{115} (His^{69} in bovine SOD) is lacking due to a deletion of seven residues in the zinc subloop (Figs. 1 and 3*B*). These mutations are conserved in the *M. leprae* and *M. avium* ssp. *paratuberculosis* sequences. Moreover, the *M. leprae sodC* gene carries also the Asp-to-Gln mutation at position 126. Two histidine residues are located in the short "zinc subloop" of *M. tuberculosis*, *viz.* His^{114} and His^{118}. His^{114} is not present in the sequences of the other mycobacteria, and the x-ray structure does not suggest any particular structural or catalytic role for this residue. His^{118}, which is too far from the redox center (~17 Å), thereby excluding any contribution to maintenance of the active site, is oriented toward the solvent and represents one of the most disordered residues in the structure. Another highly conserved residue among both eukaryotic and prokaryotic enzymes is Asp^{167} (Asp^{122} in bovine SOD). Asp^{167} is fundamental in the formation of the second coordination sphere, forming a bridge between copper and zinc ligands (His^{44} and His^{69} in bovine SOD, respectively), and is a key determinant of the active-site conformation and stability. This residue is conserved in *M. tuberculosis*, where it makes hydrogen bond contacts with the copper ligand His^{84} and with the amide nitrogen of Phe^{169}, but is far from the histidine residues corresponding to the ones coordinating zinc in the other SODs. Moreover, this residue is mutated to asparagine in *M. avium* ssp. *paratuberculosis*. Taken together, the analysis of these mutations and deletions indicates that there is no structural basis for the MtSOD enzyme to bind zinc and supports the hypothesis that the lack of zinc is a feature common to all of the mycobacterial *sodC*-encoded enzymes.

Dimer Architecture—As shown in Fig. 1, MtSOD is very similar to other prokaryotic SODs such as *A. pleuropneumoniae* SOD concerning the structural elements involved in intersubunit contacts. However, the structural comparison of the two dimers reveals completely different dimer architecture. Due to the conservation of the primary structure's special features, MtSOD, as well as all other mycobacterial SODs, is expected to have a novel dimerization interface, which can be divided into two major segments: the core Greek key β-barrel and the dimerization loop, an 18-amino acid long insertion into the eukaryotic electrostatic loop between strands 7g and 8h. The dimerization loop protrudes from the enzyme core in a direction roughly perpendicular to the β-barrel axis. The N-terminal part of the dimerization loop has a random coil structure; at its tip, it forms a short β-strand, and then it turns back toward the body of the enzyme, forming a random coil and a short helix (Fig. 4*A*).

The presence of this dimerization loop significantly increases the interface area of the MtSOD dimer compared with that of

either prokaryotic or eukaryotic SODs. Comparison of the number of polar interactions such as hydrogen bonds and salt bridges shows a striking difference between these representative SODs (Table IV). The formation of an antiparallel β-sheet at the tip and a series of polar interactions between the random coil regions of the dimerization loop evidently contribute to the elevated number of polar interaction in the dimerization interface. The increased interface area and the nearly 10-fold greater number of intersubunit hydrogen bonds in the MtSOD dimer confer a very stable quaternary structure also under physiological conditions. In analogy with the other prokaryotic Cu,Zn-SODs (30), many water molecules are trapped between the two subunits, which are further stabilized by an efficient hydrogen bonding network, in particular those that facilitate a bridge between the interface residues of the interacting monomers (Fig. 4*B*).

The dimerization loop not only increases the number and strength of the intersubunit contacts, but also changes the mutual orientation of the subunits in the MtSOD dimer compared with that in the typical prokaryotic dimer assembly, as shown in Fig. 4*B*, where one subunit of the ApSOD and MtSOD dimers is superimposed on each other. In this representation, the 2-fold symmetry axis of the ApSOD dimer is nearly perpendicular to the 2-fold symmetry axis of the MtSOD dimer, leaving the non-superimposed monomers in totally unrelated orientations. Another consequence of the shifted noncrystallographic 2-fold axis in the MtSOD dimer is the formation of a continuous *antiparallel* β-sheet made by strands 1a, 2b, 3c, and 4f contributed by both interacting subunits in the order of 1a-2b-3c-4f-4f-3c-2b-1a (Fig. 4*A*). In contrast, these strands are *parallel* in prokaryotic SODs such as ApSOD, as the 2-fold axis of the ApSOD dimer is quasi-parallel to the above-mentioned β-strands (Fig. 4*B*). In contrast, the intersubunit interactions in prokaryotic SODs do not involve main chain–main chain hydrogen bonds as found in the case of the MtSOD dimer. The interactions between the parallel β-strands are rather mediated via a number of solvent molecules (30) This extended dimer interface in MtSOD might compensate the structural stability conferred by zinc in classical Cu,Zn-SODs.

Catalytic Activity and Electrostatics of MtSOD—In the pH 6.5–7.5 range, the enzyme displays a catalytic rate ($k = 2.4 \times 10^9$ M^{-1} s^{-1}) comparable with that of several eukaryotic enzymes (41, 42), but slightly lower than that of *P. leiognathi* and *S. typhimurium* Cu,Zn-SODs (43, 19). Unlike the eukaryotic enzymes, whose activity is stable up to pH 9.0, MtSOD activity drops above pH 8.0, with an inflection point at pH ~8.5 (Fig. 5*A*). It should be pointed out, however, that a significant pH dependence of activity has already been observed in the other prokaryotic Cu,Zn-SODs from *P. leiognathi* (43) and *E. coli*.[3]

To influence the diffusion rate of the superoxide anion, both prokaryotic and eukaryotic Cu,Zn-SODs utilize electronic guidance by exploiting the electrostatic potential of positively charged residues on the rim of the active-site channel. This is achieved in prokaryotes via a cluster of lysine residues in the S–S subloop and similarly in eukaryotic enzymes, where lysine residues in the electrostatic loop serve this purpose. At the physiological ionic strength, the metal cluster and the invariant Arg^{199} (Arg^{141} in bovine numbering) are mainly responsible for the enhancement of the substrate diffusion toward the active site (44). Although there are no charged residues either in the S–S subloop or in the dimerization loop (which corresponds to the eukaryotic electrostatic loop) in the mycobacterial SODs, the active site is surrounded by an area of positive potential centered on a lysine residue (Lys^{198} in MtSOD) present in all mycobacterial SODs, which precedes the universally conserved Arg^{199} and points toward the solvent (Figs. 1 and 6). The introduction of this positively charged residue close to the entrance of the active site could functionally compensate the loss of the electrostatic loop typical of eukaryotic or Gram-negative prokaryotic enzymes.

Spectroscopic Analyses—Both absorption bands observed in the visible absorption spectrum of MtSOD (Fig. 7*A*) are due to the presence of oxidized copper and disappeared following the addition of reducing sodium dithionite. The broad band centered at higher wavelengths is characteristic of all Cu,Zn-SODs. In contrast, the presence of the 355 nm band is unprecedented in native enzymes of this class and resembles a similar absorption band observed in eukaryotic zinc-depleted enzymes (45). All Cu,Zn-SODs show a band at ~420 nm, assigned to a ligand-to-metal charge transfer transition between the imidazole of His^{61} (bovine numbering) and the copper (46). Similarly, the 355 nm band is tentatively assigned to a charge transfer process involving the imidazole ligands and copper.

The EPR spectrum of MtSOD (Fig. 7*B*), which was not affected by the addition of zinc to the protein, shows no variations up to pH values above 9.0; the significant spectral modifications observed above pH 10.5 are due to protein denaturation and are largely reversible upon lowering pH. This behavior is similar to that of classic Cu,Zn-SODs, whereas zinc-depleted eukaryotic SODs show significant alterations in the EPR spectrum above pH 6.0 (47).

The ability of MtSOD to bind zinc was tested by introducing cobalt into the demetallated protein to form a copper/cobalt-containing SOD derivative. The addition of stoichiometric amounts of copper yielded enzyme with visible and EPR spectra typical of the native enzyme. On the other hand, the subsequent addition of a 10-fold molar excess of cobalt did not influence the spectroscopic properties of the enzyme. Together, these findings suggest that the gross structural modifications of the zinc loop both preclude binding of Zn^{2+} and, at the same time, compensate for its absence.

Concluding Remarks—All known copper-containing SODs contain a zinc ion in the active site that is linked to copper via a common histidine ligand (30). Copper is the catalytic center of the enzyme and is cyclically oxidized and reduced during the successive encounters of the enzyme with the superoxide anion. In contrast, the role of zinc has not yet been completely deciphered. Zinc greatly contributes to the exceptional thermal stability of Cu,Zn-SODs (16, 48) and to their resistance to denaturing agents and proteolytic enzymes (13). Besides this structural role, however, there is also evidence that zinc modulates the reactivity of the enzyme. In fact, the removal of zinc produces pH-dependent alterations in the copper environment (47) and makes the activity of the enzyme pH-sensitive (49). Moreover, zinc-deficient Cu,Zn-SODs show an enhanced ability to catalyze the nitration of tyrosine residues by peroxynitrate (50) and are rapidly reduced by ascorbate (14, 51). Therefore, since several of the Cu,Zn-SOD mutations found in association with the familial form of amyotrophic lateral sclerosis are characterized by altered zinc binding, it has been proposed that the altered redox properties of the zinc-deficient enzyme may underlie the toxic gain of function typical of amyotrophic lateral sclerosis mutant Cu,Zn-SODs (51, 14). Finally, it should be noted that, despite noticeable differences in the modality of subunit assembly and active-site channel organization, prokaryotic and eukaryotic Cu,Zn-SODs conserve an identical arrangement of the zinc and copper ligands (30). In view of the apparent importance of zinc in all known copper-containing SODs, the discovery of a fully functional but zinc-devoid copper-containing SOD in *M. tuberculosis* was unexpected.

[3] A. Battistoni and P. O'Neill, unpublished data.

The results from the combined structural and spectroscopic analyses of MtSOD reported here indicate that this SOD lacks a zinc-binding site and suggest that the lack of zinc is compensated by significant structural modification with respect to the other enzymes belonging to the Cu,Zn-SOD family. Some clues to tentatively explain the structural evolution of mycobacterial SODs might be found in a recent study focused on the mechanisms of zinc uptake in bacteria (52). A major result of that study is that the ability of several pathogens to survive and multiply within the infected host is critically dependent on their ability to obtain sufficient amounts of zinc, as this metal is an essential cofactor of several enzymes required for bacterial growth and viability. In fact, the inactivation of bacterial high affinity Zn^{2+} uptake systems dramatically affects the ability of different pathogens to colonize the host and to cause disease (Ref. 52 and references therein). The hypothesis that zinc availability could be limited during infections is also supported by a previous study revealing that, in some pathogens, Cu,Zn-SOD is characterized by the presence of a histidine-rich N-terminal domain favoring the uptake of the active-site metal cofactors in competitive environments (53). Little is known about the mechanisms of zinc uptake in mycobacteria. However, these microorganisms reside within macrophagic phagosomes, where strong competition for transition metal binding occurs between the host and the bacterium (54).

Thus, the membrane-associated MtSOD is specifically located in a microenvironment that is likely poor in zinc. On this ground, we speculate that the structural rearrangements observed in MtSOD could be the result of selective processes aimed at obtaining a fully active enzyme relieved of the need to recruit the zinc ion within the host macrophages.

Acknowledgments—We thank Manfred Burghammer and David Flot (ID13 microfocus beamline of the European Synchrotron Radiation Facility) for great assistance during data collection. We are indebted to Dr. Janosz M. Bujnicki (International Institute of Molecular and Cellular Biology, Warsaw, Poland) for help in using the STRUCLA metaserver.

REFERENCES

1. Zahrt, T. C. (2003) *Microbes Infect.* **2,** 159–167
2. Cole, S. T., Brosch, R., Parkhill, J., Garnier, T., Churcher, C., Harris, D., Gordon, S. V., Eiglmeier, K., Gas, S., Barry, C. E., Tekaia, F., Badcock, K., Basham, D., Brown, D., Chillingworth, T., Connor, R., Davies, R., Devlin, K., Feltwell, T., Gentles, S., Hamlin, N., Holroyd, S., Hornsby, T., Jagels, K., Krogh, A., McLean, J., Moule, S., Murphy, L., Oliver, K., Osborne, J., Quail, M. A., Rajandream, M.-A., Rogers, J., Rutter, S., Seeger, K., Skelton, J., Squares, R., Squares, S., Sulston, J. E., Taylor, K., Whitehead, S., and Barrell, B. G. (1998) *Nature* **393,** 537–544
3. Nathan, C., and Shiloh, M. U. (2000) *Proc. Natl. Acad. Sci. U. S. A.* **97,** 8841–8848
4. Fridovich, I. (1995) *Annu. Rev. Biochem.* **64,** 97–112
5. Edwards, K. M., Cynamon, M. H., Voladri, R. K., Hager, C. C., DeStefano, M. S., Tham, K. T., Lakey, D. L., Bochan, M. R., and Kernodle, D. S. (2001) *Am. J. Respir. Crit. Care Med.* **164,** 2213–2219
6. Cooper, J. B., McIntyre, K., Badasso, M. O., Wood, S. P., Zhang, Y., Garbe, T. R., and Young, D. (1995) *J. Mol. Biol.* **246,** 531–544
7. D'Orazio, M., Folcarelli, S., Mariani, F., Colizzi, V., Rotilio, G., and Battistoni, A. (2001) *Biochem. J.* **359,** 17–22
8. Piddington, D. L., Fang, F. C., Laessig, T., Cooper, A. M., Orme, I. M., and Buchmeier, N. A. (2001) *Infect. Immun.* **69,** 4980–4987
9. Battistoni, A. (2003) *Biochem. Soc. Trans.* **31,** 1326–1329
10. Shi, L., Jung, Y. J., Tyagi, S., Gennaro, M. L., and North, R. J. (2003) *Proc. Natl. Acad. Sci. U. S. A.* **100,** 241–246
11. Tainer, J. A., Getzoff, E. D., Beem, K. M., Richardson, J. S., and Richardson, D. C. (1982) *J. Mol. Biol.* **160,** 287–303
12. McAdam, M. E., Fielden, E. M., Lavelle, F., Calabrese, L., Cocco, D., and Rotilio, G. (1977) *Biochem. J.* **167,** 271–274
13. Forman, H. S., and Fridovich, I. (1973) *J. Biol. Chem.* **248,** 2645–2649
14. Estevez, A. G., Crow, J. P., Sampson, J. B., Reiter, C., Zhuang, Y., Richardson, G. J., Tarpey, M. M., Barbeito, L., and Beckman, J. S. (1999) *Science* **286,** 2498–2500
15. Bordo, D., Matak, D., Djinovic-Carugo, K., Rosano, C., Pesce, A., Bolognesi, M., Stroppolo, M. E., Falconi, M., Battistoni, A., and Desideri, A. (1999) *J. Mol. Biol.* **285,** 283–296
16. Battistoni, A., Folcarelli, S., Cervone, L., Polizio, F., Desideri, A., Giartosio, A., and Rotilio, G. (1998) *J. Biol. Chem.* **273,** 5655–5661
17. Lowry, O. H., Rosebrough, N. J., Farr, L. A., and Randall, R. J. (1951) *J. Biol. Chem.* **193,** 265–275
18. Fielden, E. M., Roberts, P. B., Bray, R. C., Lowe, D. J., Mautner, G. N., Rotilio, G., and Calabrese, L. (1974) *Biochem. J.* **139,** 49–60
19. Pesce, A., Battistoni, A., Stroppolo, M. E., Polizio, F., Nardini, M., Kroll, J. S., Langford, P. R., O'Neill, P., Sette, M., Desideri, A., and Bolognesi, M. (2000) *J. Mol. Biol.* **302,** 465–478
20. Kabsch, W. (1993) *J. Appl. Crystallogr.* **26,** 795–800
21. Vagin, A., and Teplyakov, A. (1997) *J. Appl. Crystallogr.* **30,** 1022–1025
22. Perrakis, A., Morris, R. J., and Lamzin, V. S. (1999) *Nat. Struct. Biol.* **6,** 458–463
23. Murshudov, G. N., Vagin, A. A., and Dodson, E. J. (1997) *Acta Crystallogr. Sect. D* **53,** 240–255
24. Collaborative Computational Project Number 4 (1994) *Acta Crystallogr. Sect. D* **50,** 760–763
25. Laskowski, R. A., McArthur, M. W., Moss, D. S., and Thornton, J. M. (1993) *J. Appl. Crystallogr.* **265,** 283–291
26. Vaguine, A. A., Richelle, J., and Wodak, S. J. (1999) *Acta Crystallogr. Sect. D* **55,** 191–205
27. Lu, G. (1996) *Protein Data Bank Quarterly Newsletter* **78,** 10–11
28. Sasin, J. M., Kurowski, M. A., and Bujnicki, J. M. (2003) *Bioinformatics* **19,** 252–254
29. Page, R. D. (1996) *Comput. Appl. Biosci.* **12,** 357–358
30. Bordo, D., Pesce, A., Bolognesi, M., Stroppolo, M. E., Falconi, M., and Desideri, A. (2001) in *Handbook of Metalloproteins* (Messerschmidt, A., Huber, R., Poulos, T., and Wieghardt, K., eds) pp. 1284–1300, John Wiley & Sons Ltd., Chichester, United Kingdom
31. Carugo, O., and Pongor, S. (2002) *J. Mol. Biol.* **315,** 887–898
32. Carugo, O., and Pongor, S. (2001) *Protein Sci.* **10,** 1470–1473
33. Johnson, M. S., Stutclife, M. J., and Blundell, T. L. (1990) *J. Mol. Evol.* **30,** 43–59
34. Grishin, N. V. (1997) *J. Mol. Evol.* **45,** 359–369
35. Jones, S., and Thornton, J. M. (1996) *Proc. Natl. Acad. Sci. U. S. A.* **93,** 13–20
36. Cudd, A., and Fridovich, I. (1982) *J. Biol. Chem.* **257,** 11443–11447
37. Djinovic, K., Coda, A., Antolini, L., Pelosi, G., Desideri, A., Falconi, M., Rotilio, G., and Bolognesi, M. (1992) *J. Mol. Biol.* **226,** 227–238
38. Stroppolo, M. E., Nuzzo, S., Pesce, A., Rosano, C., Battistoni, A., Bolognesi, M., Mobilio, S., and Desideri, A. (1998) *Biochem. Biophys. Res. Commun.* **249,** 579–582
39. Ogihara, N. L., Parge, H. E., Hart, P. J., Weiss, M. S., Goto, J. J., Crane, B. R., Tsang, J., Slater, K., Roe, J. A., Valentine, J. S., Eisenberg, D., and Tainer, J. A. (1996) *Biochemistry* **35,** 2316–2321
40. Hough, M. A., and Hasnain, S. S. (2003) *Structure* **11,** 937–946
41. O'Neill, P., Davies, S., Fielden, E. M., Calabrese, L., Capo, C., Marmocchi, F., Natoli, G., and Rotilio, G. (1988) *Biochem. J.* **251,** 41–46
42. Getzoff, E. D., Cabelli, D. E., Fisher, C. L., Parge, H. E., Viezzoli, M. S., Banci, L., and Hallewell, R. A. (1992) *Nature* **358,** 347–351
43. Stroppolo, M. E., Sette, M., O'Neill, P., Polizio, F., Cambria, M. T., and Desideri, A. (1998) *Biochemistry* **37,** 12287–12292
44. Polticelli, F., Battistoni, A., O'Neill, P., Rotilio, G., and Desideri, A. (1998) *Protein Sci.* **7,** 2354–2358
45. Pantoliano, M. W., Valentine, J. S., Mammone, R. J., and Scholler, D. M. (1982) *J. Am. Chem. Soc.* **104,** 1717–1723
46. Pantoliano, M. W., Valentine, J. S., and Nafie, L. A. (1982) *J. Am. Chem. Soc.* **104,** 6310–6317
47. Valentine, J. S., Pantoliano, M. W., McDonnell, P. J., Burger, A. R., and Lippard, S. J. (1979) *Proc. Natl. Acad. Sci. U. S. A.* **76,** 4245–4249
48. Roe, J. A., Butler, A., Scholler, D. M., Valentine, J. S., Marky, L., and Breslauer, K. J. (1988) *Biochemistry* **27,** 950–958
49. Pantoliano, M. W., Valentine, J. S., Burger, A. R., and Lippard, S. J. (1982) *J. Inorg. Biochem.* **17,** 325–341
50. Crow, J. P., Ye, Y. Z., Strong, M., Kirk, M., Barnes, S., and Beckman, J. S. (1997) *J. Neurochem.* **69,** 1945–1953
51. Lyons, T. J., Liu, H., Goto, J. J., Nersissian, A., Roe, J. A., Graden, J. A., Cafe, C., Ellerby, L. M., Bredesen, D. E., Gralla, E. B., and Valentine, J. S. (1996) *Proc. Natl. Acad. Sci. U. S. A.* **93,** 12240–12244
52. Blencowe, D. K., and Morby, A. P. (2003) *FEMS Microbiol. Rev.* **27,** 291–311
53. Battistoni, A., Pacello, F., Mazzetti, A. P, Capo, C., Kroll, S. J., Langford, P., Sansone, A., Donnarumma, G., Valenti, P., and Rotilio, G. (2001) *J. Biol. Chem.* **276,** 30315–30325
54. Forbes, J. R., and Gros, F. (2001) *Trends Microbiol.* **9,** 397–400
55. Higgins, D., Thompson, J., Gibson, T., Thompson, J. D., Higgins, D. G., and Gibson, T. J. (1994) *Nucleic Acids Res.* **22,** 4673–4680
56. Kraulis, P. J. (1991) *J. Appl. Crystallogr.* **24,** 946–950
57. Merritt, E. A., and Bacon, D. J. (1997) *Methods Enzymol.* **277,** 505–524
58. DeLano, W. L. (2002) *PyMOL*, DeLano Scientific, San Carlos, CA
59. Baker, N. A., Sept, D., Joseph, S., Holst, M. J., and McCammon, J. A. (2001) *Proc. Natl. Acad. Sci. U. S. A.* **98,** 10037–10041